PAPER 3

# The global rain forest mapping project JERS-1 radar mosaic of tropical Africa: development and product characterization aspects

In: IEEE Transactions on Geoscience and Remote Sensing 2000. Vol. 38, No. 5, September, pp. 2218–2233.
Reprinted with permission from the publisher.

# The Global Rain Forest Mapping Project JERS-1 Radar Mosaic of Tropical Africa: Development and Product Characterization Aspects

Gianfranco De Grandi, *Senior Member, IEEE*, Philippe Mayaux, Yrjo Rauste, Ake Rosenqvist, Marc Simard, and Sasan S. Saatchi

***Abstract*—The Global Rain Forest Mapping Project (GRFM) is an international collaborative effort initiated and managed by the National Space Development Agency of Japan (NASDA). The main goal of the project is to produce a high resolution wall-to-wall map of the entire tropical rain forest domain in four continents using the L-band SAR onboard the JERS-1 spacecraft. The processing phase, which entails the generation of wide area radar mosaics from the raw SAR data, was split according to the geographic area. In this paper, the focus is on the part related to Africa. The GRFM project's goal calls for the coverage of a continental scale area of several million km$^2$ using a sensor with the resolution of tens of meters. In the case of the African continent, this entails the assemblage of some 3900 high resolution SAR scenes into a bitemporal mosaic at 100 m pixel spacing and with known geometric accuracy. While this fact opens up an entire new perspective for vegetation mapping in the tropics, it presents a number of technical challenges. In this paper, we report on the solutions adopted in the GRFM Africa mosaic development and discuss some quantitative and qualitative aspects related to the characterization and validation of the GRFM products. In particular, the mosaic geolocation and its validation are discussed in detail. Indeed, the internal geometric consistency (subpixel accuracy in the coregistration of the two dates), and the absolute geolocation (residual mean squared error of 240 m with respect to ground control points) are key features of the GRFM Africa mosaic. Other important aspects that are discussed are the multiresolution decomposition approach, which allows for tracking the evolution of natural phenomena with scale; the internal semi-automatic radiometric calibration, which minimizes artifacts in the mosaic; and the thematic information content for vegetation mapping, which is illustrated by a few examples elaborated by visual interpretation. Experience gained so far indicates that the GRFM products constitute an important source of information for global environmental studies.**

***Index Terms*—Calibration, geometric modeling, image classification, radar applications, radar cross sections, radar data processing, radar signal analysis, synthetic aperture radar (SAR), tropical regions, vegetation mapping, wavelet transforms.**

## I. Background

THE GLOBAL Rain Forest Mapping Project (GRFM) [1], [2] is an international collaborative effort initiated and managed by the National Space Development Agency of Japan (NASDA), Hatoyama. The main goal of the project is to produce a high resolution wall-to-wall map of the entire tropical rain forest domain in four continents (South America, Africa, Asia, and Australia) using the L-band synthetic aperture radar (SAR) onboard the JERS-1 spacecraft.

The adequate monitoring of Earth ecosystems is a prerequisite to the sustainable management of renewable resources. Tropical and boreal forests are a case in point because they represent important pools of economical, biological, and ecological resources. These ecosystems are furthermore threatened by the rapid increase, worldwide, in the demand for new agricultural land and for new products.

Another important aspect related to these ecosystems is their role in the exchange processes between the atmosphere and the geo-, biosphere, and in particular for the carbon cycle and for fluxes of green house gases (GHGs) such as carbon dioxide and methane. In turn, this issue is linked to global climate change, a problem of major concern for all mankind on spacecraft Earth, and hence of great political and scientific relevance. The Protocol to the U.N. Framework Convention agreed to in Kyoto, Japan, has stressed the severity of the problem and confirmed the general awareness and political will to take action toward a long term solution. The Kyoto protocol makes provision for the use of biological GHG sources and sinks to meet commitments, and understandably requires inventory of resources such as forestry and land use change as a basis on which decisions will be taken for future action to account for anthropogenic disturbances. Space provides a unique vantage point and Earth observations by satellite, a unique technology to acquire such information.

An important requirement in the case of ecosystem-wide monitoring is the combination of timeliness, completeness, and spatial resolution of the observations. The NASDA GRFM project is a possible answer to this requirement, based on the recognition that the JERS-1 L-band spaceborne SAR characteristics are ideally suited for mapping and monitoring the vegetation distribution of an entire ecosystem at continental scale, at several spatial resolutions, and with no weather or time of day constraints.

The sheer size and complexity of the project (some 13 000 radar images covering some 50 million km$^2$) demanded international cooperation from an early stage. Among the main institutions that take part in the project worldwide, we cite the Earth Remote Sensing Data Analysis Centre of Japan (ERSDAC),

Manuscript received August 31, 1999; revised April 24, 2000.

G. De Grandi and P. Mayaux are with the Joint Research Centre, European Commission, Global Vegetation Monitoring Unit, Space Applications Institute, (VARESE), Ispra, Italy (e-mail: frank.de-grandi@jrc.it).

A. Rosenqvist was with the Space Applications Institute, Joint Research Centre (JRC), Ispra, Italy, and is now with NASDA, Tokyo, Japan.

Y. Rauste was with the Space Applications Institute, Joint Research Centre (JRC), Ispra, Italy, and is now with VTT Automation, Espoo, Finland.

M. Simard and S. Saatchi are with the Jet Propulsion Laboratory, Pasadena, CA 91109 USA.

Publisher Item Identifier S 0196-2892(00)08911-7.

0196–2892/00$10.00 © 2000 IEEE

Tokyo, Japan, the National Aeronautics and Space Administration (NASA), Washington, DC, the Jet Propulsion Laboratory (JPL), Pasadena, CA, the Alaska SAR facility (ASF), Fairbanks, AK, the European Commission Joint Research Centre (EC JRC), Ispra, Italy, the National Institute for Space Research of Brazil (INPE), São Jose Dos Campos, Brazil, the National Institute for Amazonian Research of Brazil (INPA), Manaus, Brazil, and the University of California, Santa Barbara (UCSB).

Certainly, this strategic vision, which brought together the expertise of major space-related institutions in Japan, the U.S., and Europe and the knowledge and skills of scientists all around the world, was one of the major assets that assured the so far very successful outcome of the project. The GRFM is also, in our opinion, a good example of how the study of global environmental problems requires a concerted effort at the international level.

The project includes a technology part related to the satellite operations, data acquisition and processing for the generation of the wide area radar mosaics, and a science program to support global or local area thematic studies of the tropical ecosystems. As far as the technology part is concerned, the following task structure and allocation was adopted. The SAR data downlink and correlation was performed at the NASDA Earth Observation Center, Hatoyama, Japan, and at the ASF, Fairbanks, Alaska. The latter effort was funded by NASA.

The SAR high resolution detected images were then distributed to a number of main processing nodes for the postprocessing phase involving low resolution product generation and wide area radar maps compilation, suitable for further automatic processing and thematic information extraction. The load was shared according to a geographic area criterion. The South America data set was assigned to the Jet Propulsion Laboratory, California Institute of Technology (funded by NASA), the Africa data set to the EC JRC Space Applications Institute (SAI), the Asia and Australia part to NASDA Earth Observations Research Center EORC. Each center was responsible for developing its own processing algorithms and software, since due to the project's requirements no off the shelf solution was available.

In this paper, the focus is on the Africa postprocessing part of the GRFM project. The postprocessing baseline product consists of a georeferenced, calibrated, bitemporal SAR wide area mosaic at 100 m pixel spacing, comprising radiometric and textural information. Additional products are also generated including multiresolution maps and texture measures (from 200 m down to 1.6 km). In particular, we will describe the main technical and engineering issues of the processor that was developed for the generation of the GRFM Africa products and will discuss some quantitative and qualitative aspects related to the characterization and validation of the products.

The paper is structured as follows. In the next section, we highlight the project's main characteristics and novel aspects. The generation of the Africa mosaic products entails several data sets, software and hardware components, that we collectively indicate as the Africa mosaic engine. These components are described in Section III. In Section IV, a statistical characterization of some baseline products is given. The next Section V deals with the core issue of the mosaic compilation and georeferencing, with particular emphasis on the geometric validation process (Section VI). In Section VII, the problem of correcting radiometric distortions is tackled. In Section VIII, we give a first assessment of the mosaic information content *vis-a-vis* the theme of tropical vegetation mapping. This step, which is conducted at this stage by visual inspection, is an important prerequisite to characterize the potential of the GRFM products for future automatic classification pursuits. Finally, we summarize the current status of the project and hint at the ongoing and future activities within the GRFM Africa project.

## II. Project's Highlights

The GRFM approach calls for the coverage of a continental scale geographic area (a linear distance of some 6000 km in the case of the Africa mosaic) using a SAR sensor which acquires a scene within a swath of some 75 km and with a ground resolution of approximately 18 m. This is obtained by tiling together several acquisitions which are not taken instantaneously but still within a short time frame (two months). Moreover due to the orbital characteristics of the JERS-1 spacecraft contiguous swaths are imaged within two consecutive days, which assures a smooth time evolution through the whole coverage.

The resulting product is a spatially continuous radar map, which can eventually be degraded to lower resolutions for studying scale dependent natural phenomena, or to extract thematic information at the most suitable resolution. In the case of the tropical ecosystems, the merit of the approach lies therefore in the possibility of estimating some geophysical parameters of interest (e.g., biomes distribution, deforestation) globally and at unprecedented resolution.

Previous approaches relying on optical sensors were either producing wide area continuous sampling but low resolution maps (e.g., the EC Tropical Ecosystem Environment monitoring by Satellites TREES project vegetation maps based on NOAA AVHRR 1 km data [3]) or high resolution but random coverage data sets [4]–[6] (e.g., LANDSAT TM data). In this case, some global geophysical parameters were then estimated by extrapolation using statistical sampling techniques.

The combination of continuous coverage, short acquisition time, and high resolution is a unique asset of the GRFM approach. Experience gained so far lets us confidently say that data sets such as the GRFM ones will bring forth entirely new paradigms for the remote sensing of wide area terrestrial phenomena and will add enormously to our knowledge of the tropical and other poorly documented earth ecosystems. However the benefit comes at the cost of a number of technical hurdles.

First the end to end process from the satellite down link to the generation of several layers of lower resolution products entails a staggering data volume, and a high processing complexity. Experience in handling large data volumes was certainly not lacking among the major GRFM processing nodes. For instance, a wide area radar mosaic of Central Africa using the ESA ERS-1 SAR data had already been generated at the JRC SAI [7]. Still, the GRFM project introduced one more shift in complexity, due to the geographically distributed processing, and the layers of low resolution products (multitemporal, multiresolution). To give a flavor, the GRFM Africa mosaic consists of some 3900 SAR scenes which is tantamount to 312 Gb of high

resolution ground range data, and 4.8 Gb for one 100 m baseline product, without accounting for all the intermediate and special purpose lower resolution products. This level of data volume already poses some problems even for simple operations like data ingestion if the available off-the-shelf computer technology in the high end Unix servers and workstation class is used.

Second, since the coverage is not obtained in one snapshot, perturbation of the imaging system nominal values (e.g., the satellite attitude) affect the images that compose the mosaic according to their position differently (e.g., radiometric and geometric distortions). These effects must be taken in due account and corrected for. Moreover, the problem of parameters estimation is exacerbated by the data volume issue, because most manual techniques, like tie-pointing, must be ruled out.

Third, even a self-consistent measure of a physical parameter still requires a comparison with independent estimates to be validated. Validation of the image characteristics and, as a second step, of the thematic information that can be eventually extracted (e.g., a vegetation map), is in our opinion one of the central issues in the generation and exploitation of wide area high resolution remote sensing data sets. The validation of a measurement that is spatially dependent and extends over a wide area requires a reference set of known and suitable accuracy and must be dense enough to assure the correct sampling of the signal to validate. The problem is compounded by the fact that ad hoc ground experiments are nowadays difficult to set up in areas of the world like Central Africa, which are plagued by high social and political unrest. Historical data sets are in this case the only source for benchmarks.

In the context of the GRFM Africa postprocessing the validation of the georeferencing accuracy was of particular relevance, because clearly it constitutes a prerequisite to the use of the GRFM radar maps for cartographic applications. These peculiar connotations needed to be taken into account in the GRFM development process and constituted the rationale for the development of suitable processing techniques and tools, which are reported in this paper.

## III. The GRFM Africa Mosaic Engine

The GRFM Africa processing chain can be seen from a purely computational point of view as an ensemble of data sets and processes that perform a transformation from the input data sets (the JERS-1 imagery supplied by NASDA) to the output data sets, which are referred to as the GRFM Africa multiresolution products. We indicate this ensemble of data sets, software, and the hosting hardware devices as the "GRFM engine." In this section, we give an overview of the engine main components and their interactions (see diagram in Fig. 1).

### A. Input Data Sets

The JERS-1 SAR data acquisitions of the GRFM Africa project include two blanket coverages of the Central Africa tropical region between 10°S and 10°N. The first coverage was acquired during January–March 1996 and extends from 8°E to 42°E. The second during October–November 1996 and extends from 8 to 36°E. In the following, the two data sets will be dubbed the "low water" and "high water" data sets, with reference to the perceived

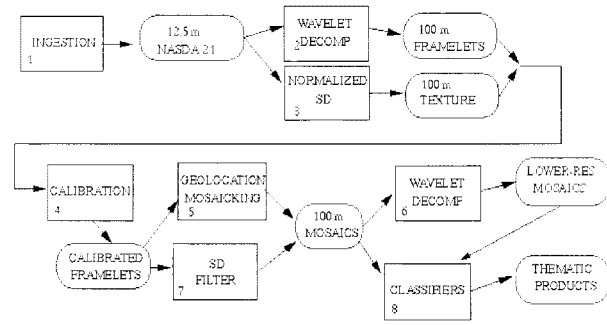


Fig. 1. Diagram of the main components of the GRFM Africa processing chain. The ensemble of the hardware, software processes (square boxes), the digital products (curved boxes), and their interconnections (arrows) is referred to as the GRFM Africa engine. The main processes are numbered for reference in the description of the data flow given in Section III.

hydrological state of the main river network in the region, the Congo river and its tributaries. In addition, the low water data set covers West Africa from 14°W to 8°E and the island of Madagascar (acquired on January 1997).

The SAR raw data corresponding to these acquisitions were correlated at NASDA Earth Observations Center EOC. The output of this processing phase is a product defined by NASDA as a standard geocoded image in a Universal Transverse Mercator (UTM) projection and dubbed Level 2.1 product. However, the rows and columns of the Level 2.1 raster file are aligned with the slant range and azimuth directions and not with the Mercator reference system.

The low water acquisition comprises 2173 scenes, the high water acquisition 1460 scenes in continental Africa, and 263 scenes for the Madagascar island. All the scenes were acquired on descending orbits.

### B. Data Flow

Proper management of the data flow in terms of hardware resource allocation, operation synchronization, and housekeeping information is an issue of primary importance in a complex processing system like the GRFM one. Typically the following data flow takes place. The NASDA level 2.1 high resolution images are ingested in batches into the system. The data ingestion step is the most time critical in the overall chain of operations; in our configuration it required approximately two calendar months for all the GRFM data sets.

The high resolution data are then processed by the wavelet decomposition block (block 2 in Fig. 1 and Section III-C), which generates images and texture measures downsampled at 100 m. This product is the basic building block for all successive operations needed to build the mosaic. Products at this resolution will be called framelets.

The framelets are radiometrically calibrated (block 4 in Fig. 1) and geolocated and tiled together (block 5 in Fig. 1). This step produces the baseline products at 100 m resolution (bitemporal mosaics and texture measures).

Larger scale (lower resolution) maps and texture measures are generated again by wavelet decomposition from the baseline products (block 6 in Fig. 1). The multiscale radiometric and texture products are finally used to support further analysis, data

distribution, visual interpretation, and automatic thematic information extraction (block 8 in Fig. 1).

### C. Wavelet Multiresolution Decomposition

A multiresolution signal decomposition based on the wavelet transform is used to generate the GRFM Africa products. The rationale for using this approach instead of a classical downsampling method such as block averaging, stems from several considerations.

1) Multiresolution is an intrinsic concept in the wide area radar mapping approach, where a high resolution sensor is used for wide area mapping. The wavelet pyramid gives the possibility of generating approximations of the original radar imagery at several spatial scales (at each stage in the pyramid, the pixel size is double with respect to the previous level). Therefore, it is possible to generate a set of products that best match the thematic analysis requirements for a certain application in terms of resolution, SNR, and data volume.
2) The wavelet coefficients at a scale $j$ carry information on the "details" of the signal that were present in the approximation at a finer scale $j-1$ and were lost in the approximation at scale $j$. The wavelet coefficients can therefore be interpreted as texture measures at that scale and the wavelet decomposition provides at the same time the approximated image, and information on spatial structures that exist in the image at a certain scale. This fact opens up several possibilities for the automatic extraction of structural and textural information [11], a definite advantage over other multiresolution techniques.
3) The existence of fast discrete wavelet transform algorithms, which require only a number of operations proportional to the size $N$ of the original data, makes this approach ideal in the case of high data volume (in contrast for instance, fast Fourier transforms (FFTs) are typically $N \log N$ algorithms).

The basic theory behind the wavelet based decomposition used in the GRFM engine was developed by Mallat [8]. Details on the adaptation of the theory in the case of SAR imagery and multiplicative speckle noise and on the retrieval of textural and singularity information can be found in [9]–[13].

### D. Multiresolution Products

The wavelet decomposition generates from each high resolution level 2.1 image and for each scale three products: 1) the smooth signal; 2) the wavelets coefficients (horizontal, vertical, oblique); and 3) the scalogram. The scalogram at scale $j$ as defined in [10] is the quadratic sum of the wavelet coefficients normalized by the squared smooth signal at that scale to compensate for the wavelet amplitude modulation due to multiplicative speckle noise in stationary areas. Scalograms are useful for constructing multiscale texture maps [11].

It is important to notice that the low pass and high pass filters in the decomposition are applied after a square law detector. In this way, over stationary areas, the intensity mean value is preserved after low pass filtering and therefore, an unbiased estimation of the radar backscattering coefficient is still possible at higher scales (lower resolution).

In parallel to the main pyramid another texture measure product is generated by computing the normalized standard deviation (sample standard deviation normalized by the sample mean) $SD_N$ of the high resolution amplitude signal over contiguous blocks of $8 \times 8$ pixels. This texture measure is intuitively proportional to the one point signal variations (namely independent of the spatial ordering) within a resolution element of 100 m. For an homogeneous area with constant underlying radar reflectivity, they are entirely due to speckle noise. $SD_N$ will therefore assume the nominal value for a 3-look amplitude image with correlated fully developed speckle. Deviations from this nominal value indicate that other variations are occurring in the signal within the 100 m resolution cell. See the next section for some statistical considerations on this texture measure.

It is important to realize that the normalized standard deviation $SD_N$ is complementary and bears different information with respect to the wavelet scalogram $SW^j$. The scalogram at resolution $j$ contains the details that were lost from the higher resolution $j-1$ in approximating the signal, and therefore contains variations that were detectable at scale $j-1$ but that were wiped out at scale $j$. For instance, $SW^j$ at 100 m contains textural information at the 50-m scale. By contrast, the $SD_N$ measure contains texture at all scales from 12.5 m up to 100 m.

## IV. Statistical Considerations

### A. Speckle Strength in the Low Resolution Products

The baseline radiometric products at 100-m pixel size are derived from the high resolution level 2.1 data by low pass filtering, the intensity signal, and by decimation. Speckle noise, which is present in the original data, will therefore be attenuated at larger scales but still be present. This has to be taken into account in the development of postprocessing analysis tools such as classifiers and edge detectors.

A quantitative estimation of the speckle strength for a stationary area with fully developed correlated speckle can be obtained considering a simple theoretical model. In the discrete wavelet decomposition, the two-dimensional (2-D) smooth signal at each scale is generated by convolution with a separable (rows and columns) low pass filter and by decimation. Relationships between the input and output random processes statistical parameters (expectations and correlation functions) at each stage in the decomposition can be obtained using the theory of stable, time-invariant linear filters.

Assuming that at the first stage (highest resolution), the input signal $x$ will be correlated only up to 1 lag, the normalized second moment of the output process $z$ can be expressed as

$$m_2(z) = m_2(x)c^2[0] + 2c[1]m_2(x) \cdot (\rho_r c[0] + \rho_a c[1]) + 2(c[0]+1)\sum_{l=2}^{\infty} c[l] \qquad (1)$$

where

$m_2(x) = (E[x^2]/E^2[x])$ normalized second moment of the random process $x$ and indicator of the speckle strength;

$c[l]$ autocorrelation sequence of the wavelet low pass filter impulse response;

$\rho$ normalized autocovariance at 1 lag.

Typical values for JERS-1 level 2.1 data are $\rho = 0.355$ in azimuth and $\rho = 0.4$ in range.

Since the decimation process after both convolutions (by rows and columns) decorrelates the signal, we can assume white speckle noise from the second scale downward. Then, cascading $n$ such filter stages, a relationship between the normalized second moment $m_2[x]$ at the input of the wavelet decomposition and the normalized moment $m_2[x_n]$ at stage $n$ can be obtained

$$m_2[x_n] = m_2[x]c^{n-1}[0] + 2\sum_{l=1}^{\infty} c[l] \sum_{k=0}^{n-2} c^k[0]. \quad (2)$$

Since there are two filters in the decomposition the scale level $s$ is linked to $n$ by $n = 2s+1$. Substituting numerical values for the low pass filter coefficients used in the wavelet decomposition in (1) and (2) and considering at the input a stationary random process drawn from intensity data with an equivalent number of looks $ENL = 2.6$ (as in a level 2.1 product), we obtain at the output of the pyramid $ENL = 59$ for the 100 m product and $ENL = 154.2$ for the 200 m product. For comparison a block average of $8 \times 8$ pixels would generate a product at 100 m pixel size with $ENL = 46.6$.

### B. Variance of the Normalized Standard Deviation Estimator

We now turn to the statistical characterization of the texture measure based on the normalized standard deviation of the high resolution level 2.1 amplitude data. As explained in Section III-D, a local estimator is implemented in the GRFM processing by computing the sample normalized standard deviation of the data (three looks, 12.5 m pixel size) using an N × N window. The window is moved blockwise in the image.

This estimator turns out to be a good discriminator for some thematic forest classes of interest such as the swamp and the lowland rain forest, because it is sensitive to the upper canopy structure. It is therefore important to estimate the variance of the estimator in order to assess the SNR (or in other words the class separability).

The estimator can be expressed as a function of the statistics $T_1$ and $T_2$

$$S\hat{D}_n = \frac{\sqrt{\frac{1}{N}\left(\sum_i (x_i - \overline{x})^2\right)}}{\frac{1}{N}\left(\sum_i x_i\right)} = g(T_1, T_2) \quad (3)$$

$$T_1 = \frac{1}{N}\left(\sum_i x_i^2\right), \quad T_2 = \frac{1}{N}\left(\sum_i x_i\right) \quad (4)$$

where $x_i$ are the observations and in this case, the amplitude values of the level 2.1 radar image.

Performing a first order Taylor expansion around the mean values $\overline{T}_1$ and $\overline{T}_2$, we have [14]

$$\begin{aligned}\operatorname{var}\left(S\hat{D}_n\right) = {} & \operatorname{var}(T_1)\left(\frac{\partial g}{\partial T_1}\right)^2_{T_1=\overline{T_1}} \\ & + \operatorname{var}(T_2)\left(\frac{\partial g}{\partial T_2}\right)^2_{T_2=\overline{T_2}} \\ & + 2\operatorname{cov}(T_1, T_2)\left(\frac{\partial g}{\partial T_1}\right)_{T_1=\overline{T_1}}\left(\frac{\partial g}{\partial T_2}\right)_{T_2=\overline{T_2}}.\end{aligned} \quad (5)$$

Equation (5) can be expanded as a function of the moments of the observables $x_i$, of the estimation window size, and the of normalized autocovariance function of $x$ at 1 lag. All of these quantities can be computed from a theoretical probability distribution function and a correlation model of the SAR data. A detailed derivation is given in [25].

Numerical evaluation of (5) for $K$-distributed 3-looks amplitude data as a function of the order parameter $\nu$ of the $K(\nu, \overline{I})$ distribution and the estimator window size gives the results reported in Table I.

For a stationary area with Rayleigh or K-distributed speckle, the expected value of $S\hat{D}_n$ is a constant, which we consider the signal. The noise component is due to the estimator variance. In this sense, the standard error in Table I can be interpreted as the SNR of the texture measure. This analysis indicates how an improvement of the S/N can be traded off against the spatial resolution. Alternatively, the texture measure signal can be filtered to improve the SNR before the classification engine.

The theoretical estimator variance is the basis for the construction of such a filter (block 7 in Fig. 1). The filter uses the local statistics in the neighborhood of a pixel in the image to detect stationary areas where the statistical regime described above is present. This is achieved using the theoretical estimator variance (5) as a function of the mean value. If the variance threshold is exceeded, an adaptive window algorithm is entered, similar to the one proposed in [15]. If a stationary area is not detected even at this second level, then the original value is stored in the filtered set. Otherwise, the local sample mean is substituted for the current pixel.

The scope of the filter is therefore to smooth the texture measure in stationary areas with constant or Gamma distributed radar cross section and to preserve fine and strong features in nonstationary areas of the texture signal.

## V. Geolocation

The geolocation of the individual scenes (framelets) is a fundamental step in the mosaic compilation. The problem can be explained as follows. If each framelet were to be positioned in a Mercator reference system relying only on the scene coordinates given in the NASDA product ancillary data, geometric inconsistencies would arise with respect to other framelets. Points belonging to the same feature on the ground would be displaced as seen in a framelet or in a neighboring one. This is due to errors in the sensor's position and uncertainty in the estimation of the Doppler centroid frequency that propagate in the solution of the range Doppler equations used by NASDA to rectify the geolocated level 2.1 product. The standard deviation of the

TABLE I
THEORETICAL VARIANCE OF THE SAMPLE ESTIMATOR $S\hat{D}_n$ (NORMALIZED STANDARD DEVIATION) FOR AMPLITUDE STATIONARY $K$-DISTRIBUTED SAR DATA AS A FUNCTION OF THE ORDER PARAMETER $\nu$ OF THE $K(\nu, \bar{I})$ DISTRIBUTION. THE ESTIMATOR VARIANCE AND STANDARD ERROR ARE REPORTED FOR AN ESTIMATOR MOVING WINDOW OF 8 × 8 PIXELS AND 16 × 16 PIXELS

| | | 8x8 window | | 16x16 window | |
|---|---|---|---|---|---|
| $S\hat{D}_n$ | ν | $\sqrt{var(S\hat{D}_n)}$ | Std. Error% | $\sqrt{var(S\hat{D}_n)}$ | Std. Error% |
| 0.30 | 77.68 | 0.037 | 12.34 | 0.019 | 6.27 |
| 0.35 | 7.66 | 0.042 | 12.12 | 0.021 | 6.15 |
| 0.40 | 3.80 | 0.047 | 11.99 | 0.024 | 6.07 |

scene geolocation data was experimentally estimated to be several hundreds of meters, and discontinuities of up to 600 m were detected. On the other hand, internal geometric consistency and between dates coregistration of the mosaics for the multitemporal analysis require that the location accuracy of individual scenes is better than the pixel dimension (100 m). Methods for revising the geolocation data must therefore be applied in the mosaic compilation. A global optimization technique was developed based on a linear least squares estimation (LLS) of the scene geometry parameters given observations that comprise interscenes correlation measures, ground control points, and nominal scene position. The two acquisitions at different dates are simultaneously included in the estimation process, thus assuring optimal coregistration between dates.

From an intuitive point of view, the internal mosaic geometric consistency would be assured if the same features in different neighboring images were to match perfectly. Now the same feature on the ground is indeed imaged twice in the overlap area of two adjacent framelets. This fact can be exploited to get a measure of the relative discrepancies in the positions of the two framelets. The next problem is to move one framelet relative to the other in such a way as to be consistent with the positions of the other neighboring framelets and to avoid the propagation of errors in one direction as a function of the order in which the relative displacements are considered. The solution is to look for a global minimization of all the observed discrepancies.

This kind of global optimization technique has been studied in an application area of linear algebra which is called the calculus of observations [17]. The principle that underpins the calculus of observations can be summarized as follows. Suppose we experimentally perform M observations (e.g., coordinates of a point $P$ in two images) that are linked to $N$ parameters to be adjusted by a linear system of equations. In matrix form, $Ax + b = 0$, where $x$ is a vector of $N$ parameters, and $A$ is an $M$ by $N$ matrix.

If no error were present in the observations the linear system would be consistent. Otherwise, we would have a discrepancy $\delta = Ax + b$ that we would want to minimize in the least square sense. This requires [17] that $\delta^T\delta$ be a minimum or

$$\frac{\partial}{\partial x}\left(\delta^T\delta\right) = 2A^TAx - 2A^Tb = 0. \tag{6}$$

These are the so-called normal equations and can be solved for the parameters vector $x$ if the $N \times N$ matrix $A^TA$ is nonsingular. Weighting factors can be also introduced in the error criterion $\delta^T\delta$ in order to emphasize the samples that are deemed more reliable. Then the error to be minimized becomes $\delta^TW\delta$, where $W$ is a positive definite $N \times N$ weighting matrix.

The application of this global optimization technique to the case of image block adjustment requires the definition of a geometric model or in other words the definition of the observation equations $\delta = Ax + b$. We use a model [18] where, given a framelet in the Mercator projection, the scene center translation $\nabla N_C \nabla E_C$ and the rotation angle $\alpha$ are considered as parameters. This model relies on the confirmed assumption that there is no internal deformation in the NASDA level 2.1 products. Working the problem in a conformal mapping projection minimizes the risk of introducing projection-dependent systematic deformations. Also, the rotation angles are kept small and therefore, the block adjustment can be simplified by linearizing the observation equations.

With the aid of an auxiliary reference system with origin at the scene center, the relationship in the Mercator reference system between one point P in the image and the unknown parameters can be derived where

$$\begin{aligned} N^P &= N_C + y\cos\alpha - x\sin\alpha \\ E &= E_C + x\cos\alpha + y\sin\alpha \end{aligned} \tag{7}$$

$N^PE^P$ Mercator coordinates of point $P$;
$x, y$ image coordinates in the auxiliary reference system and $N^CE^C$ are the coordinates of the scene center;
$\alpha$ rotation angle of the auxiliary system with respect to the Mercator system.

The observations equations $\delta = Ax + b$ based on tie-points between scenes are

$$\begin{aligned} \delta N^P &= N_1^P - N_2^P = N_1^C - N_2^C + y_1\cos(\alpha_1) \\ &\quad - y_2\cos(\alpha_2) - x_1\sin(\alpha_1) + x_2\sin(\alpha_2) \end{aligned} \tag{8}$$

$$\begin{aligned} \delta E^P &= E_1^P - E_2^P = E_1^C - E_2^C + x_1\cos(\alpha_1) \\ &\quad - x_2\cos(\alpha_2) - y_1\sin(\alpha_1) + y_2\sin(\alpha_2). \end{aligned} \tag{9}$$

These equations are put into the suitable linear form in the parameters $N_1^CN_2^CE_1^CE_2^C\alpha_1\alpha_2$ by a Taylor's series and retaining only first order terms. Thus, for example for the Northing term

$$\begin{aligned} \delta N^P &= f\left(N_1^C, N_2^C, \alpha_1, \alpha_2\right) \\ &= \delta N_0^P + \nabla N_1^C - \nabla N_2^C + \frac{\partial f}{\partial \alpha_1}\nabla\alpha_1 + \frac{\partial f}{\partial \alpha_2}\nabla\alpha_2 \end{aligned} \tag{10}$$

where

$\nabla N_1^C \nabla N_2^C$ translations in Northing of the scene;
$\alpha_1\alpha_2$ rotations of the scenes with respect to their local reference systems;
$\delta N_0^P$ initial Northing discrepancy at point $P$.

The elements of the matrix A in the observations equations are the partial derivatives with respect to the parameters, and the vector $b$ corresponds to the initial discrepancies before the adjustment. Tie-point measurement is based on image correlation performed at 100 m pixel spacing between adjacent scenes belonging to the same date mosaic or between scenes at two different dates. For scenes acquired along the same orbit, the correlation peak is well defined even without high contrast features. Even homogeneous areas can be correlated successfully,

because the same speckle pattern is present in both scenes. The points within one date and between strips always require the presence of a high contrast feature that remains stable during the interval between the SAR acquisitions of the adjacent strips. The same applies to the points between flood season, but here the overlap area to search for candidate features is larger because the scenes (same node or path-row position) cover the same area.

Measurements related to tie points between two neighboring scenes assure only control over the internal consistency and the coregistration of the bitemporal mosaic. However, in order to improve the absolute geolocation accuracy also ground control points (GCPs) derived by external cartographic data were introduced. In this case, the observation equations for a GCP of known geodetic coordinates $N_{true}E_{true}$ are

$$\begin{aligned}\delta N^P &= N^P_{computed} - N^P_{true} \\ &= N^C + y\cos\alpha - x\sin\alpha - N^P_{true} \end{aligned} \tag{11}$$

$$\begin{aligned}\delta E^P &= E^P_{computed} - E^P_{true} \\ &= E^C + x\cos\alpha + y\sin\alpha - E^P_{true}. \end{aligned} \tag{12}$$

Finally, information on the image location derived from the SAR ancillary data was added to the LLS adjustment. This last information is by far less accurate than the one derived by tie points between images but is still useful in establishing a bound on image rotation and translation with respect to the original position.

The structure of the LLS normal equations coefficient matrix $N = A^T W A$ is block diagonal with bandwidth

$$w = (2s_{path} + 1) \cdot n_{dates} \cdot n_{par} \tag{13}$$

where

- $s_{path}$ maximum number of scenes in a single path (fast row index);
- $n_{dates}$ number of dates (SAR coverage);
- $n_{par}$ number of parameters in the geometric model.

A conjugate gradient method [19] can be used efficiently for the solution of linear systems with a block diagonal coefficient matrix. In the case of the bitemporal Africa mosaic, the matrix size is 10 875 × 10 875, which is also an indicator of the processing complexity.

## VI. Geolocation Validation

In order to validate the georeferencing accuracy, a sequence of block adjustments using different sources for the observations in the LLS were performed, and the relative residual mean square errors (RMSE) measured. The hierarchy of tests included: 1) observations based only on tie-points between neighboring scenes; 2) additional observations based on GCPs located on the coast lines; and 3) additional observations based on GCPs located in the interior of the continent. All three adjustments included 3624 scenes and 62 006 tie-points.

Digital data from the World Vector Shoreline data base was used for the GCPs along coastlines. The World Vector Shoreline data covers fairly well West Africa, the Western coastal zone of Africa down to Angola, and the part of the Tanzanian–Kenyan coast that is included in one of the mosaics. Digital topographic maps with scale 1 : 200 000 in the Central African Republic and the Republic of Congo (Congo/Kinshasa) were used in test case 2. The maps were produced by IGN/France mainly in the 1950s. The maps were scanned and digitized by I-Mage Consult, Namure, Belgium within the framework of the Regional Environmental Information Management Project on Central Africa (REIMP-CA), initiated under the PRGIE program of the Worldbank.

TABLE II
Residual Mean Square Error (RMSE) Statistic in the GRFM Geolocation Block Adjustment. All Quantities are in Meters. Centre $N$ And Centre $E$ are Scene Translations in Northing and Easting. The Column Mean $\nabla N$ And Mean $\nabla E$ Give the Average Relative Translations Between the Two Dates Mosaics. Ground Control Point (GCP) $N$ And GCP $E$ are the Coordinates of the Ground Control Points

| *Test case* | *Tiepoint N* | *Tiepoint E* | *Centre N* | *Centre E* | *GCP N* | *GCP E* | *Mean* $\nabla N_{1,2}$ | *Mean* $\nabla E_{1,2}$ |
|---|---|---|---|---|---|---|---|---|
| 1 | 33.2 | 34.8 | 477.5 | 751.7 | 503.0 | 1021.4 | 26.6 | -289.7 |
| 2 | 35.5 | 40.8 | 532.0 | 736.2 | 193.7 | 201.6 | 18.6 | -69.3 |
| 3 | 40.1 | 39.7 | 543.3 | 758.0 | 173.2 | 166.3 | 24.3 | -46.8 |

Results of the validation process are reported in Table II. The table gives RMS errors in meters for various quantities of interest. The columns *Centre N*, *Centre E* are scene translations in Northing and Easting. The column *Mean* $\nabla N_{1,2}$, *Mean* $\nabla E_{1,2}$ give the average relative translations between the low water and the high water mosaics. The RMS error on GCP's in case 1 indicates the error computed when the 248 coastline GCPs are not included in the LLS adjustment but only used to estimate the error.

As to case 2, the inclusion of GCPs in the least squares estimation LLS degrades the tie-points RMSE by a few meters. On the other hand, it greatly reduces the discrepancy between the mosaic and external control data (from 500 m to less than 200 m in Northing and from 1000 m to less than 200 m in Easting). In case 3, about 50 GCPs located in the Central African Republic and the Republic of Congo were added to the observations, but the RMSE statistic of scene translation vectors did not change significantly. From this fact we can infer that these GCPs are compatible with the coast line GCPs at the scale of the mosaic pixel size (100 m).

In case 1, the GCP data were a completely independent test set. In the error analysis of cases 2 and 3, the same GCP data set is used both to derive the parameters of the model and to test the accuracy of the model. Theoretically, a better error estimate could be obtained using an independent test set. However, to the best of our knowledge, no such set exists for tropical Africa given the error budget and extension required. One solution could have been to divide the GCP population into two sets (one for model derivation and the second for testing), alternating for instance 500-km stretches along the coast line for each set. This approach was not followed for two reasons. First, it was thought that RMS errors of the order of 200 m are already close or below the accuracy specification of the vector shore line data (dividing the population into two sets would still give the same level of RMS errors). Second, the splitting could introduce systematic errors (as a result of differences in origin and quality of the map material used to derive the coast line data) into the analysis depending on the way the partitioning is made.

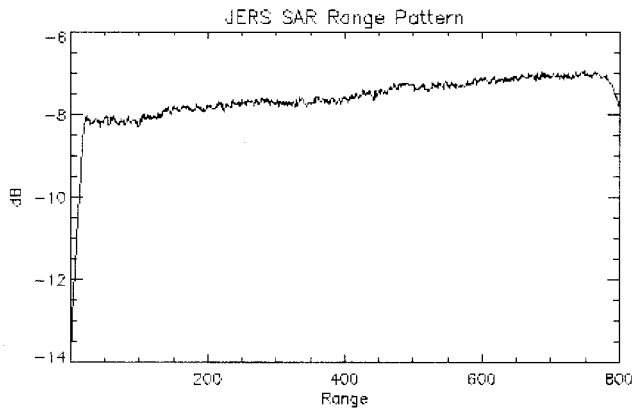


Fig. 2. Typical JERS-1 level 2.1 product range pattern (average backscatter amplitude as a function of the range coordinate). Notice the anomalous behavior where the backscatter increases from near to far range. This pattern cannot be expected for any natural target and is therefore a processing artifact probably due to the sensor's attitude variations. However, since the artifact manifests itself randomly in the set of images composing the mosaic and cannot be characterized by analysis of the SAR ancillary data, an empirical calibration algorithm had to be devised that relied on a global minimization of radiometric discrepancies between the same ground target imaged in two neighboring images.

## VII. Radiometric Calibration

### A. Calibration Algorithm

The calibration of most spaceborne SAR sensors is based on the use of the tropical forest as a calibration target [20], [21]. Usually the antenna pattern, determined on the ground before the launch of the satellite, is revised based on the fact that the backscattering coefficient $\gamma^\circ$ of the tropical forest is constant over a wide range of incidence angles. The revised antenna pattern is then used in connection with SAR processing to produce calibrated SAR products. This approach works well if all the necessary spacecraft (such as platform attitude angles) and processing parameters remain constant or are known with the required accuracy. Uncontrolled drift in these parameters may cause changes in the SAR range pattern and degrade the (relative) calibration accuracy.

Indeed the main calibration artifact that pollutes the JERS-1 level 2.1 products is related to the average backscatter amplitude as a function of the range coordinate in homogeneous areas. In many scenes, the range pattern shows an anomalous behavior whereby the average amplitude increases from near range to far range (see Fig. 2). Typically, the increase is of 1 dB across the image swath. This kind of backscatter curve cannot be expected for natural targets.

Other radiometric problems in the JERS-1 imagery are related to striping in the along track direction due probably to errors in processing the sensitivity time control (STC) data and between scenes gain imbalance.

Since the reasons for these calibration artifacts are not known, and related characterization data cannot be deduced from the header data of the SAR level 2.1 products, an empirical method based on backscatter estimates of the same target in neighboring scenes was devised to remove the artifacts. Also, the procedure requires a minimum amount of manual intervention, a relevant factor in the GRFM Africa context, where a large number of scenes acquired at different times must be processed.

The resulting calibration should be considered accurate only in flat areas. Indeed due to the unavailability of suitable digital elevation models at continental scale in the Africa tropical region, techniques to compensate radiometric errors due to the influence of topography were ruled out. Also, since topography is not accounted for, the term "incidence angle" in the following must be understood under the assumption of flat terrain.

The automatic calibration procedure is based on the following rationale. The dominant land cover type in the area covered by the GRFM project is tropical rain forest. Scatterometer measurements at C-band [20] indicate that this natural target exhibits a constant backscattering coefficient $\gamma^\circ$ over 50° incidence angle range from 18 to 68°. The same results are confirmed at L-band for the JERS-1 SAR in [21]. For the 4° incidence angle range used (96% of the mosaic pixels have an incidence angle between 37.4 and 41.5° due to the overlap between strips and the far-range-on-top mosaic compilation mode), it is safe to assume that also other land cover types with rough surfaces such as dry wood, land, or open-canopy forest (savanna), have a practically constant $\gamma^\circ$.

Assuming a constant $\gamma^\circ$ for major land cover types over the range of incidence angles means that a pixel observed at far-range incidence angle and near-range incidence angle in an overlap area between strips should have the same backscattering value in both strips provided that no environmental change has influenced the backscatter level between the two acquisitions. Due to its unique orbit, the JERS-1 radar acquired the two adjacent strips on two consecutive days. Therefore, it is reasonable to assume that the $\gamma^\circ$ of an overlap area remains the same in the relatively weather-insensitive L-band SAR data.

The objective of the calibration procedure is to produce mosaics with minimum radiometric difference between scenes in the overlap areas (and consequently along the seams between scenes), both within a strip and between strips.

This is achieved by using an LLS of the coefficients in a bilinear radiometric correction model

$$DN_{cal} = (1 + f_0 + f_1 x + f_2 y + f_3 x \cdot y) \cdot DN_{orig} \quad (14)$$

where $x$, $y$ are normalized line and columns coordinates derived from the line and column indices in the SAR image.

The model incorporates a constant gain factor and coordinate dependent gain factors. The main part of the calibration artifact is a function of the range coordinate only (see Fig. 2). Since the reason for this artifact is not known, it cannot be assumed that the calibration artifact would remain constant as a function of time. Azimuth and cross terms are therefore included in the radiometric correction model.

Points in the overlap area between two neighboring scenes are used to derive observations for the LLS adjustment. The observation equation for two scenes is

$$\begin{aligned}\delta = {} & f_0^2 DN_{orig2} + f_1^2 DN_{orig2} \cdot x \\ & + f_2^2 DN_{orig2} \cdot y + f_3^2 DN_{orig2} \cdot xy \\ & - f_0^1 DN_{orig1} - f_1^1 DN_{orig1} \cdot x - f_2^1 DN_{orig1} \cdot y \\ & - f_3^1 DN_{orig1} \cdot xy + DN_{orig2} - DN_{orig1} \end{aligned} \quad (15)$$

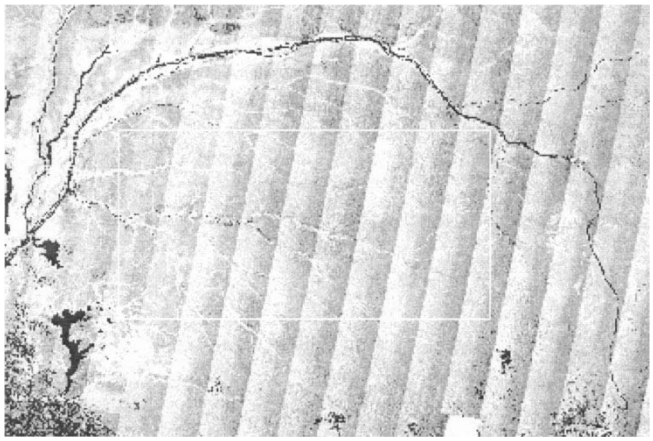

(a)

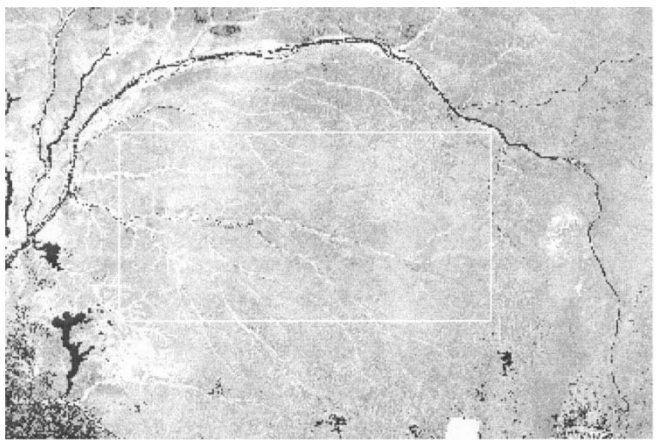

(b)

Fig. 3. (a) Subset of the high water mosaic compiled using the original, noncalibrated 100-m framelets. The effect of the anomalous range pattern is clearly visible and produces what could be called a striping effect in the image. (b) The same mosaic after the bilinear LLS calibration revision. Clearly, the major calibration artifacts have been removed.

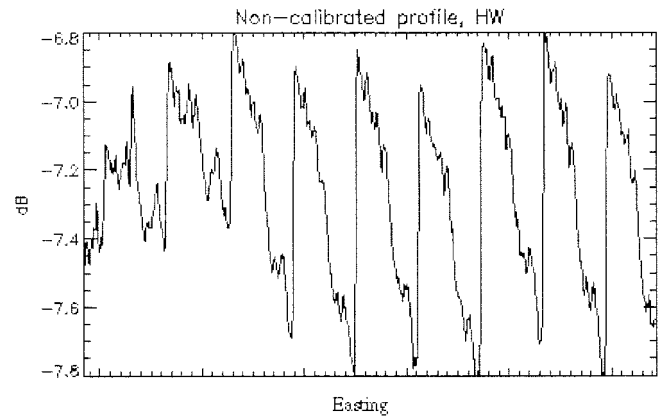


(a)

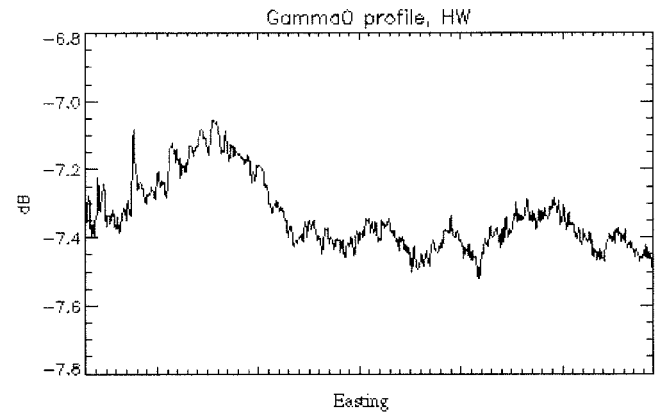


(b)

Fig. 4. (a) Average range profile computed on the noncalibrated mosaic in the window highlighted in Fig. 3. There is a pronounced increase if 1 dB in the backscatter over the image swath. (b) The average range profile of the calibrated image confirms that the calibration artifacts have been corrected for.

where $f_j^i$ is the correction factor for image $i$ and order $j$, and $DN_{orig1}DN_{orig2}$ are digital values of image 1 and 2 in the overlap area.

### *B. Calibration Results*

This section reports on sample results of the GRFM calibration procedure. A subset of the high water mosaic composed using the original uncalibrated 100-m scenes is shown in frame a) of Fig. 3. An average profile computed over the rectangle highlighted in Fig. 3 is plotted in frame a) of Fig. 4. This profile was computed projecting each pixel to an Easting coordinate along lines parallel to the orbit direction. Because the look direction of JERS-1 in descending orbits is westwards, the range coordinate decreases with increasing Easting coordinate. This graph clearly indicates that there is a pronounced increase of almost 1 dB over the image swath.

The same mosaic subset compiled using the calibrated framelets and the associated range profile are shown in frame b) of Figs. 3 and 4. The calibration anomaly (increasing backscatter with increasing range) has been clearly compensated for.

Analysis of the calibration results for the bitemporal mosaics confirms that the method works in a satisfactory way using automatic (systematic grid sampling) selection of calibration points in forested areas. However in very dynamic environments such as flooding in savanna or in grassland areas, the backscatter may change considerably even during the one-day interval between the acquisition of adjacent strips. These cases can be detected by careful inspection of the calibration factors, and must be handled by a separate semiautomatic procedure. This procedure calls for the removal of the automatically selected calibration points and the interactive selection of points in areas which can be expected to be less prone to meteorological changes in backscatter level (e.g., the primary rain forest).

The GRFM calibration method produces a constant response backscatter curve which corresponds to the constant $\gamma^\circ$ in forested areas. The calibration coefficient (in the near-range far-range direction) does not change notably when going from a forest area into a savanna area. This confirms the assumption that the backscatter coefficient $\gamma^\circ$ of savanna can also be considered as constant over the incidence angles present in the mosaic.

Finally, one comment should be made regarding the possibility of retrieving $\sigma^\circ$ values form the DN values of the Africa mosaics. The assumptions made in the radiometric model for the

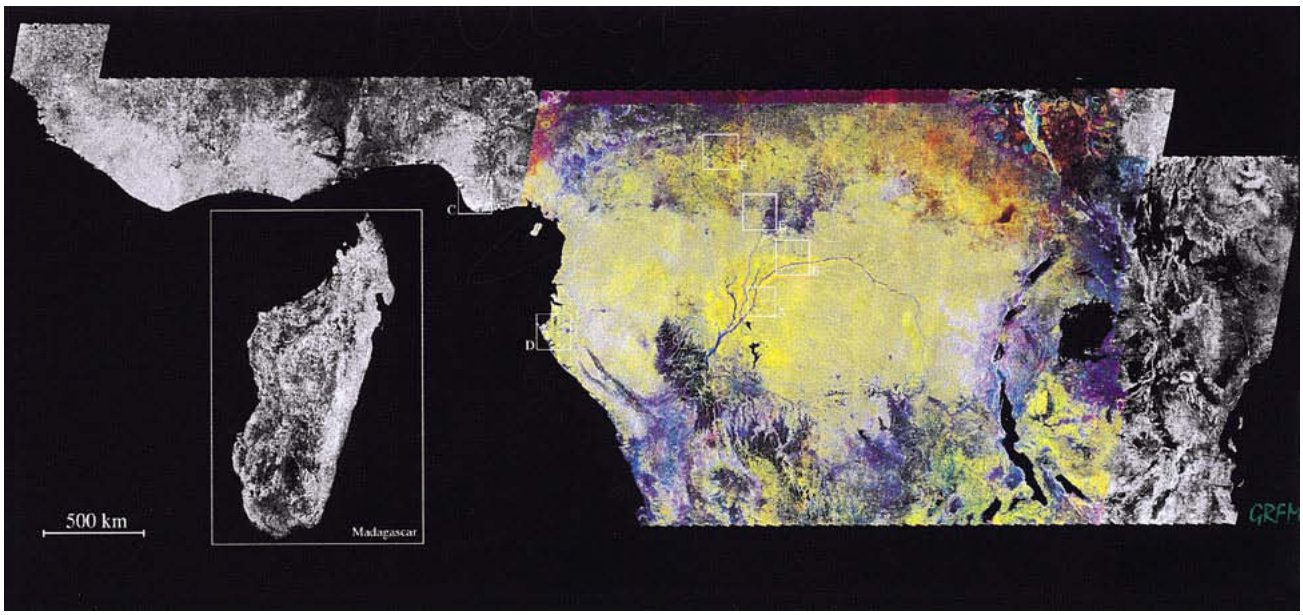


Fig. 5. Synoptic view of the GRFM Africa mosaic. The mosaic extends from the western coast of Africa in Sierra Leone at 14° W to the eastern coast in Kenya and Tanzania at 42° E in longitude and from 10° S to 10° N in latitude. In addition, the island of Madagascar is included (see inset). A blanket coverage of the whole area was acquired in January–March 1996 during the low water season of the Congo river. A second acquisition from 8° E to 36° E was also performed during the high water season in October–November 1996. The area covered by the two acquisitions is shown in false color in the figure. Areas of interest for relevant thematic features are highlighted and enlarged in the next figures.

calibration algorithm, and the several steps needed to compensate for various radiometric artifacts in the NASDA products, suggest (to be on the safe side) the disclaimer that the GRFM Africa mosaic is not suitable for building a radar cross section map. Rather, it is an internally consistent image (an approximation of the radar reflectivity) that is useful as input to supervised classification algorithms, which rely on relative comparisons of the local image amplitude statistics and texture measures.

In particular cases, such as for areas belonging to the lowland rain forest, it is safe to derive estimates of the $\gamma^{\circ}$ coefficient from the local statistics of intensity data. Knowledge of the local incidence angle would then allow for the retrieval of $\sigma^{\circ}$ values in dB using for instance the equation supplied by NASDA [21].

## VIII. Thematic Information Content

The richness in information content is one of the most striking assets of the GRFM Africa wide area radar mosaics. From the first analyses based on visual interpretation, a series of features related mainly to vegetation regional mapping and landcover change studies have already emerged and indicate that these radar maps are of great interest for global vegetation mapping, a major objective of research programs such as the International Geosphere Biosphere Programme (IGBP) and the Global Observation of Forest Cover (GOFC).

In order to give evidence about this statement, a few examples of the thematic content derived by visual inspection of the GRFM products will be reported in the following. A synoptic view of the Africa mosaic derived from the 100 m digital image is shown in Fig. 5.

The colored area corresponds to the bitemporal coverage. Already at this scale it is evident how the mosaic represents a unique cross section of important tropical biomes from the savannah and dry forest in the north through the entire rain forest domain and again through the seasonal formations south of the equator (savannah and edge of the Miombo woodland). The coverage of the mosaic is such that, since it crosses the equator, it contains at the same time dry and rainy season acquisitions with a gradient of wetness in between [23]. This allows a range of observations to be made with respect to the occurrence or to the lack of seasonal contrasts between various vegetation formations.

Areas related to the cases that are discussed are highlighted in the synoptic view and enlarged in the next series of figures.

The first case is related to the swamp forests in the Congo river floodplain. Swamp forests are interesting ecosystems that function as water storage, faunistic and florensis habitat, and fish stock. Moreover, they host a series of biochemical processes such as nitrogen turnover and methane emission. Since methane is a greenhouse gas, this process has a significance in global change issues [24]. Due to the density of the hydrographic network, swamp forests cover large areas in the center of the Congo basin, leaving room for the lowland rain forest in the inter fluvial areas only.

Different types of swamp forests coexist according to the frequency and the duration of the flooding, and they can be discriminated in the radar image by textural and radiometric differences. The L-band SAR onboard the JERS-1 satellite offer unique characteristics to map these ecosystems [25], [26]. Indeed, electromagnetic waves at L-band can penetrate even through the thick closed canopy of the Africa swamp forests and the backscattered signal is thus sensitive to standing water on the terrain through a double bounce scattering mechanism. The upper canopy of the swamp forest is closed and very homogeneous, and the radar reflectivity from direct backscattering

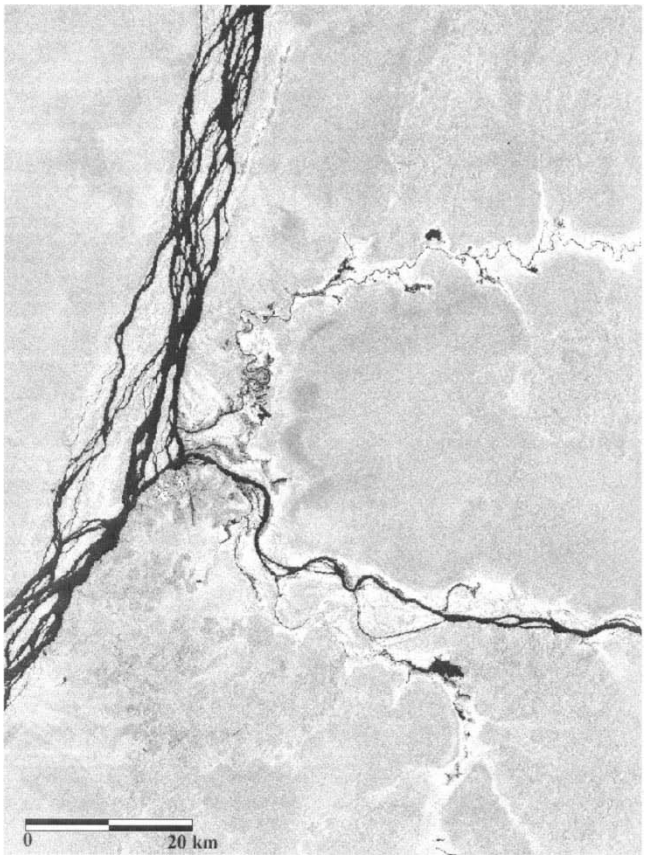


Fig. 6. Flood plains along the Congo river in Central Africa are covered by forests adapted to the soil conditions (area A in Fig. 5). As an example, in this figure, permanently inundated forests are characterized by a brighter tone (strong backscatter due to the double bounce mechanism) because of the presence of standing water. Smooth texture allow us to the distinguish periodically inundated forests to the west of the Congo River or in the large patches at the center of the image.

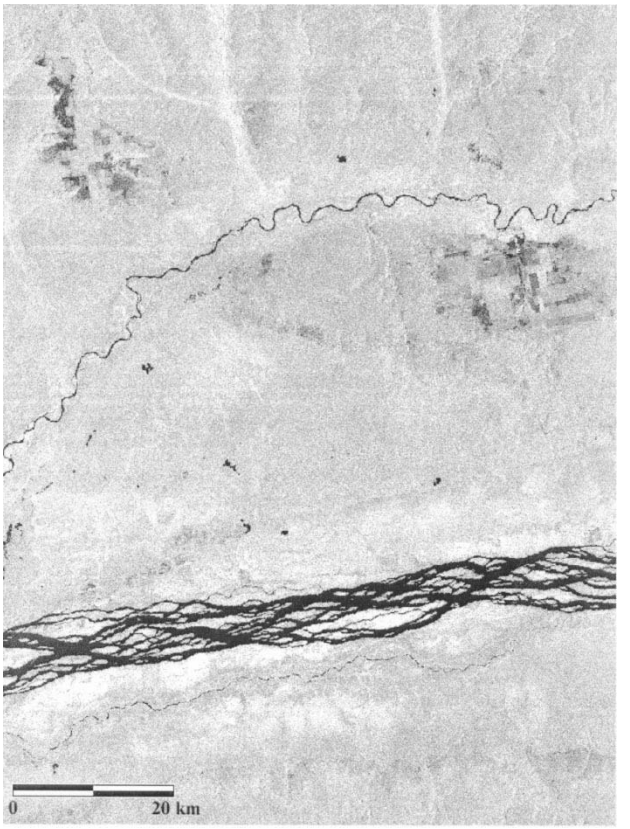


Fig. 7. Large industrial plantations (Hevea, Elaeis) established in colonial times in the proximity of the Congo River and his tributaries are readily detectable in this image due to their regular geometric shape (area B in Fig. 5). The dense network of the Congo River (lower part of the image) is very sharply delineated. The flooded swamp forests are also visible along the river due to the high double-bounce return.

exhibits smooth textural properties (statistically it approximates very well the fully developed speckle Rayleigh regime). On the other hand, species heterogeneity and a higher fragmentation modulates the spatial variations of the thick upper canopy in the lowland rain forest. This produces a microtopography effect that changes the textural properties of the radar backscatter even at L-band. An example is shown in Fig. 6.

Permanently inundated forests are characterized by brighter tone in the image (strong backscatter) because of the presence of standing water. Smooth texture permits the distinction of periodically inundated forests at the west of the Congo River or in the large patches at the center of the image.

Fig. 7 reveals the presence of large industrial plantations (Hevea, Elaeis) established in colonial times in the proximity of the Congo River and his tributaries.

The plantations are characterized by a uniform cover and follow a geometrical layout, clearly identifiable on the center and the right center of the image. The different backscatter responses correspond to different practices used in the plantation management (mainly fires). The dense river network and the numerous branches of the Congo River are very clearly delineated in the image. The capability of monitoring the river configuration, which undergoes continuous modifications, is of primary interest for the local economy of the many villages and settlements along the Congo river.

Coastal ecosystems are the target of ecological pressures by several anthropogenic activities: urbanization, oil extraction, fishing, forest logging, and hunting. In Fig. 8, the Niger Delta is shown. This area is covered by a dense network of mangroves. Mangroves are forest formations associated with marine alluvium, partially steeped in salt water. The survey of the mangrove degradation is particularly crucial in this region where many oil-extraction activities are under way and cause soil pollution.

The coastal part of Gabon, namely the city of Port-Gentil (Fig. 9), is also a site with intensive offshore oil extraction activities. The Ogooué river estuary is covered by a complex of swamp grasslands with gramineae and Papyrus, mangroves and swamp forests, lagoons and coastal savanna, and rain forests.

The city of Bangui in Central African Republic is located on the Oubangui river at the border between the savanna and the forest domains. It is clearly visible as a strong scatterer in Fig. 10. The urban expansion has a major impact since the 1960s on the forest degradation taking place toward South from the city, as attested by many openings in the forest (dark tone in the image). On the other side of the Oubangui river, a reticulated network of gallery forests penetrates into the savanna domain.

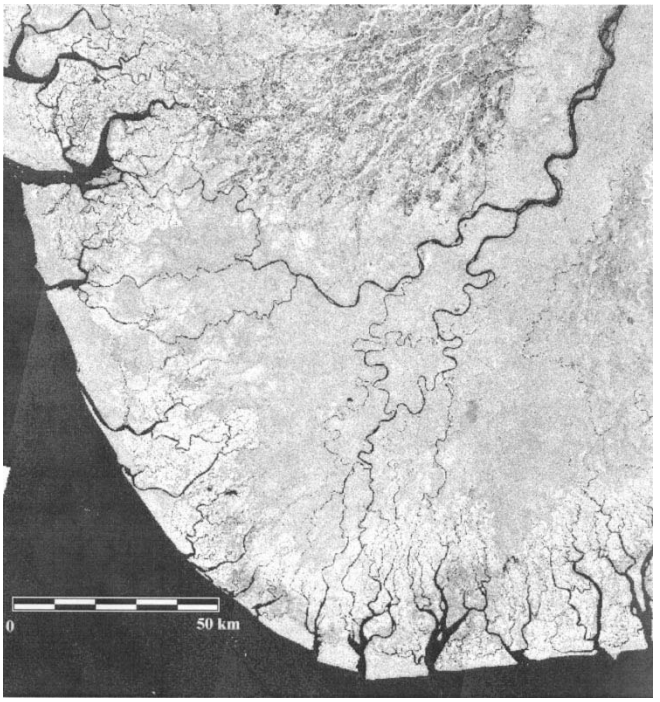


Fig. 8. The Niger Delta is a coastal ecosystem that is the target of ecological pressures by several anthropogenic activities (area C in Fig. 5). This area is covered by a dense network of mangroves (in light gray), easily distinguishable from the surrounding rain forests. A wide ribbon of dense rain forest extends along the Niger River at the North of the image in the middle of savanna and secondary zones. Note the presence of offshore platforms (bright dots in the sea).

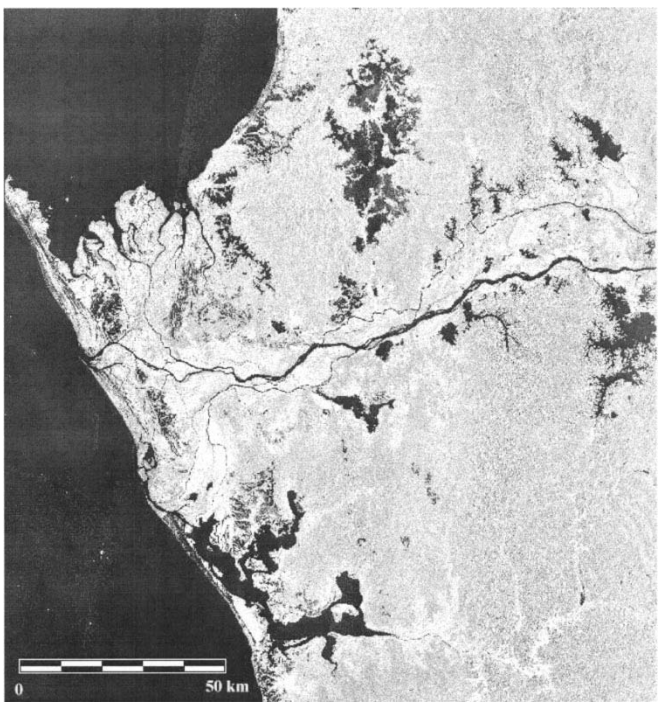


Fig. 9. The Ogooué river estuary, near by the city of Port-Gentil (area D in Fig. 5), is covered by swamp grassland, mangrove, and swamp forests (bright return). Lagoons and coastal savanna appear in black, while rain forests present an intermediate reflectivity.

These gallery forests play a key role in the biodiversity conservation.


Fig. 10. The city of Bangui in the Central African Republic is located on the Oubangui river at the border between the savanna and the forest domains and is clearly visible in this image as a strong scatterer. On the other side of the Oubangui river, a reticulated network of gallery forests penetrates into the savanna domain.

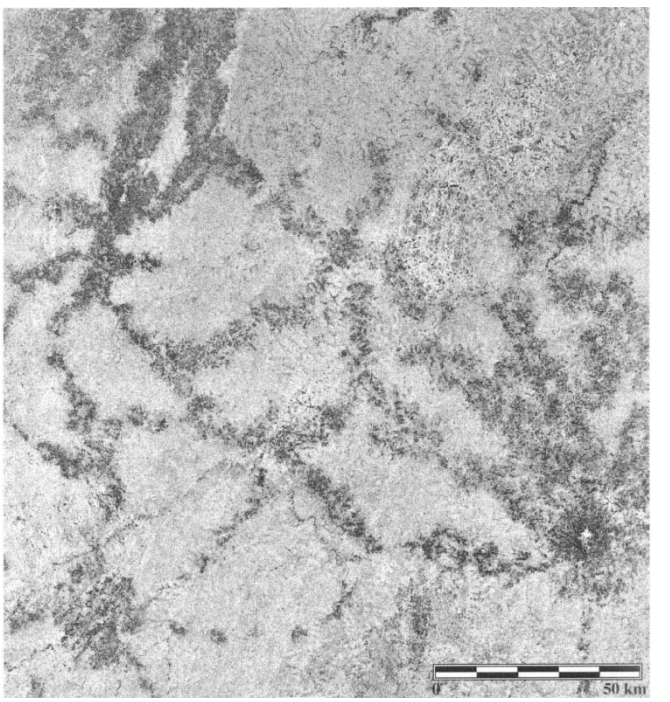


Fig. 11. A reticulated pattern of agricultural fields within the woodland and tree savanna domain in the central part of the Central African Republic.

Fig. 11 shows a reticulated pattern of agricultural fields within the woodland and tree savanna domain in the central part of the Central African Republic.

The relatively low population is concentrated along the road network. Common crops are cassava, maize, and peanuts used

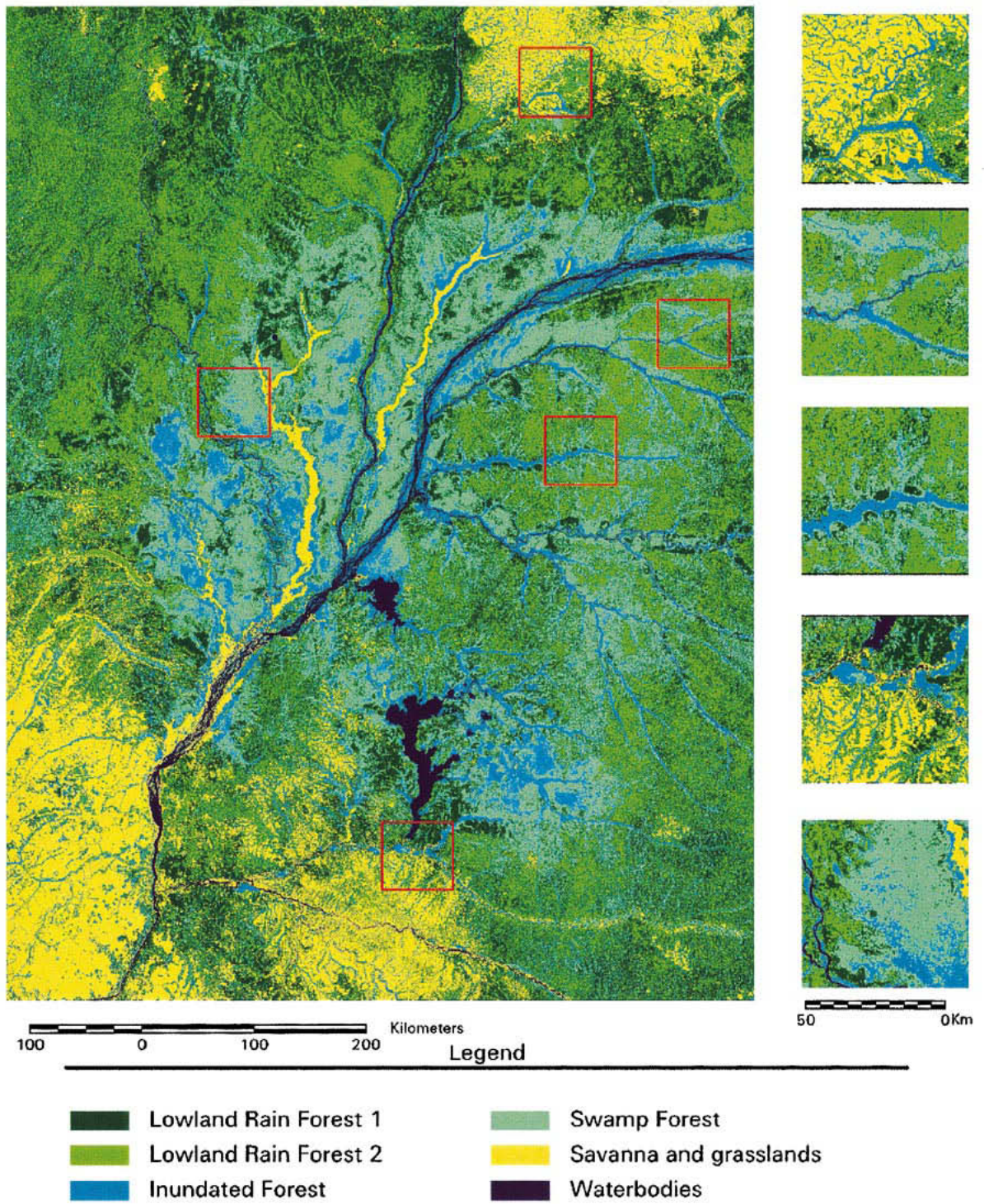


Fig. 12. Classification map of the entire Congo river floodplain at 200 m pixel size. The map was generated from the GRFM Africa high water data set (radiometry and texture) using a maximum likelihood classifier and by stratification with the TREES project GIS data. The insets show the reticulated pattern of gallery forests penetrating into the savanna domain at the south and north of the Congo basin and the presence of swamp forests in the depressions.

locally as food source and cotton for export trading. These fields with bare soil or low biomass vegetation exhibit lower L-band backscatter than the surrounding areas with higher biomass trees. In the northeast area of the picture, very dark patterns correspond to a region with more intensive agricultural practices due to the presence of a development project.

Derivation of regional scale vegetation maps from the GRFM mosaics calls for automatic thematic information extraction techniques. In this direction the first attempts using a simple supervised classification have already produced very promising results. As an example, a thematic map of the swamp and lowland rain forest in the entire Congo river basin at 200 m pixel size is reported in Fig. 12.

The map constitutes a significant update in the information on biomes like the swamp forests in the Congo floodplain that were thus far not well documented at a continental scale. Validation

of the classification accuracy, a topic of central importance in continental scale studies, is under way and will be reported in a future paper.

## IX. Summary and Future Perspectives

We have given on overview of the main technical aspects related to the compilation and the validation of the wide-area radar map of the tropical forest domain in Africa, an effort which is part of the GRFM Project.

The most salient characteristics of the GRFM Africa mosaic can be summarized as follows.

- Multitemporal and continental scale data set: Continuous coverage of tropical Africa at two dates from the west coast in Sierra Leone to the east coast in Kenya and Tanzania, covering a distance of some 6000 km, was obtained by the assemblage of more the 3900 JERS-1 SAR scenes.
- Multiresolution approach: Generation of a pyramid of products (reflectivity and texture maps) at different spatial resolutions to accommodate the needs of different types of thematic analyses. Starting from the NASDA level 2.1 SAR images at 12.5 m pixel size, the baseline mosaics are generated at 100 m pixel size, and lower resolution maps at dyadic scales down to 1.6 km.
- High internal geometric consistency of the mosaics: A multitemporal block adjustment algorithm based on tie-pointing between neighboring images gives a figure of 56 m for the RMSE. This also means that coregistration at subpixel accuracy is achieved between the two dates.
- Validated absolute geolocation accuracy: Using ground control points derived from the World Vector Shoreline data in the block adjustment and in the validation process a RMSE of 240 m was measured. This absolute geolocation accuracy probably constitutes a first in wide area radar mapping.
- Revised radiometric calibration to minimize artifact: A semiautomatic calibration method is applied in the mosaic compilation process to correct radiometric artifacts introduced mainly by the sensor's attitude errors. Although the mosaic cannot be considered a radar cross section map, it is still an approximation of the radar reflectivity suitable for the generation of thematic products either by visual interpretation or by automatic supervised image classification.
- Richness in thematic information content: Thanks to the characteristics of the JERS-1 L-band radar a number of very important features of great importance for land applications such as vegetation mapping, geomorphology, and cartography can be readily delineated in the GRFM Africa mosaics. This puts this product in a firm position for its exploitation in global environmental studies.
- Breadth of scope: The breadth of scope of the project, due to the intrinsic global (at ecosystem level) nature of the target and the involvement of several partners in a large international collaborative effort has brought forth several added value consequences. Among these are the arousal of the remote sensing community's awareness and consensus on the potential of wide area high resolution radar mapping for global environmental studies, the development of advanced processing methods, the establishment of a common technological platform through the shared experience of the involved partners, which will be the basis for bridging the GRFM approach over to future pursuits, with more global and operational characteristics.

The GRFM Africa project is now entering a second phase where the focus is on geophysical parameters retrieval and in general on automatic thematic information extraction. Other avenues currently being explored are the fusion with the ERS-1 C-band Africa mosaic and with other optical sensors' data sets. On the other hand, development of more sophisticated classification techniques that would fully exploit the multiresolution properties of the GRFM mosaics is under way, in particular at JPL. The reader is referred to [27], [28] for some preliminary results.

The GRFM Africa data set represents a milestone in wide area radar mapping of the Earth's ecosystems. However, at this stage, it is a foundation whose value will be fully exploited only if on top of it, geoscience applications will be developed by the science community at large for providing adequate information on local and global environmental issues to the policy and decision makers. In this perspective, the availability of the GRFM present and future products will be a key asset. In response to these requirements, a CD-ROM set with the GRFM Africa baseline products is already available for distribution to interested parties.

## Acknowledgment

The authors would like to thank NASDA for their fundamental role in the GRFM project, a role that unfolded from the vision of new ways and avenues for the utilization of the JERS-1 capabilities back in 1995 at the time of the project conception through a continuous and excellent technical support at all stages: spacecraft operation, data processing, and the support to the science program through a very generous data distribution policy. All the NASDA staff involved in GRFM is credited with the successful outcome of the project. In particular, we would like to thank T. Tanaka, former NASDA EORC Director, M. Shimada, Chief Architect of the NASDA SAR processing chain, A. Rosenqvist, former GRFM Manager at NASDA. They can probably be considered the project's fathers, together with A. Freeman and B. Chapman of NASA JPL. The authors would also like to thank the Technical Staff involved in GRFM, JRC SAI Global Vegetation Monitoring Unit GVM, and at NASA JPL, who played different, but equally important, roles in the project. In particular, they would like to thank P. Siqueira, NASA JPL, for his suggestions on the block adjustment algorithm, T. Richards, TREES Information System Manager, for his contribution to the geolocation, G. Perna and E. Franchino, A. Tournier, U. Costantini, B. Glenat of the GRFM Africa Software Development Team, P. Janvier for the GIS technology, F. Achard, TREES Project Manager, A. Belward, GVM Unit Manager, and R. Winter SAI Director. They would also like to thank J. M. Gregoire, E. Bartholome, JRC GVM, and M. Leysen, Flemish Institute of Technological Research, for their help in the GRFM thematic validation, and F. Holecz and P. Pasquali, formerly with the Remote Sensing Laboratories University of Zuerich, now with SARMAP Switzerland, for their contribution to the calibration algorithms.

Finally, they would like to thank J. P. Malingreau, the man whose vision was instrumental back in 1994 in setting up the whole wide area radar vegetation mapping activity at the JRC GVM. The anonymous reviewers are also thanked for their valuable suggestions and comments.

## REFERENCES

[1] A. Rosenqvist, "The global rainforest mapping project by JERS-1 SAR," *Int. Archives Photogramm. Remote Sensing*, pt. B7, vol. 31, pp. 594–598, 1996.

[2] A. Rosenqvist, M. Shimada, B. Chapman, A. Freeman, G. F. De Grandi, S. Saatchi, and Y. Rauste, "The global rain forest mapping project—A review," *Int. J. Remote Sensing: Special Issue on Global and Regional Land Cover Characterization from Satellite Data*.

[3] P. Mayaux, F. Achard, and J. P. Malingreau, "Global tropical forest area measurements derived from coarse resolution satellite imagery: A comparison with other approaches," *Environ. Conservation*, vol. 25, no. 1, pp. 37–52, 1998.

[4] D. Skole and C. Tucker, "Tropical deforestation and habitat fragmentation in the amazon: Satellite data from 1978-1988," *Science*, vol. 260, pp. 1905–1910, 1993.

[5] J. P. Malingreau and C. Tucker, "Large scale deforestation in the southern amazon basin of Brazil," *Ambio*, vol. 17, pp. 49–55, 1988.

[6] P. Mayaux, G. F. De Grandi, and J. P. Malingreau, "Central Africa forest cover revisited: A multi-satellite analysis," *Remote Sens. Environ.*, vol. 71, pp. 183–196, 2000.

[7] G. F. De Grandi, J. P. Malingreau, and M. Leysen, "The ERS-1 central Africa mosaic: A new perspective in radar remote sensing for the global monitoring of vegetation," *IEEE Trans. Geosci. Remote Sensing*, vol. 37, pp. 1730–1746, May 1999.

[8] S. G. Mallat, "A theory for multi-resolution signal decomposition: The wavelet representation," *IEEE Trans. Pattern Anal. Machine Intell.*, vol. 11, p. 674, July 1989.

[9] S. G. Mallat and W. L. Hwang, "Singularity detection and processing with wavelets," *IEEE Trans. Inform. Theory*, vol. 38, no. 2, pp. 617–642, March 1992.

[10] M. Simard, G. F. De Grandi, K. P. B. Thomson, and G. B. Benie', "Analysis of speckle noise contribution on wavelet decomposition of SAR images," *IEEE Trans. Geosci. Remote Sensing*, vol. 36, pp. 1953–1962, Nov. 1998.

[11] M. Simard, G. F. De Grandi, and K. Thomson, "Adaptation of the wavelet transform for the construction of multi-scale texture maps of SAR images," *Can. J. Remote Sensing*, vol. 24, pp. 264–285, Sept. 1998.

[12] M. Simard, G. F. De Grandi, S. Saatchi, M. Leysen, and K. P. B. Thomson, "Processing and analysis techniques for continental scale radar maps of the tropical forest," in *Proc. IEEE IGARSS'97 Symp.*, Singapore, 1997, pp. 1890–1892.

[13] F. De Grandi, J. S. Lee, D. Schuler, G. Kattenborn, F. Holecz, P. Pasquali, and M. Simard, "Singularity analysis with wavelets in polarimetric SAR imagery for vegetation mapping applications," in *Proc. IEEE IGARSS'99*, Hamburg, Germany, 1999, Paper E05-06.

[14] S. M. Kay, *Fund.Statistical Signal Processing*. Englewood Cliffs, NJ: Prentice-Hall, 1993, pp. 294–299.

[15] J. S. Lee, "Refined filtering of image noise using local statistics," *Comput. Graph. Image Processing*, vol. 15, pp. 380–389, 1981.

[16] A. V. Oppenheim and R. W. Schafer, *Discrete Time Signal Processing*. Englewood Cliffs, NJ: Prentice-Hall, 1989, pp. 63–67.

[17] L. Mirsky, *An Introduction to Linear Algebra*. New York: Dover, 1990, p. 156, 158.

[18] Y. Rauste, T. Richards, G. F. De Grandi, G. Perna, E. Franchino, and A. Rosenqvist, "Compilation and validation of the GRFM Africa SAR mosaics using multi-temporal block adjustment," *JERS-1 Sci. Prog. 99 PI Reps., NASDA EORC*, pp. 99–108, Mar. 1999.

[19] W. H. Press, B. P. Flannery, S. A. Teukolsky, and W. T. Vetterling, *Numerical Recipes in C: The Art of Scientific Computing*. Cambridge, U.K.: Cambridge Univ. Press, 1992, pp. 84–85.

[20] P. Lecomte and E. Attema, "Calibration and validation of the ERS-1 wind scatterometer," in *Proc. First ERS-1 Symp. Space at the Service of our Environment*, Cannes, France, Nov. 4–6, 1992, pp. 19–29.

[21] M. Shimada, "Radiometric and geometric calibration of JERS-1 SAR," *Adv. Space Res.*, vol. 17, no. 1, pp. 79–88, 1996.

[22] A. H. Devol, J. E. Richey, W. A. Clark, and S. L. King, "Methane emissions to the troposphere from the Amazon floodplain," *J. Geophys. Res. 93*, pp. 1583–1592, 1998.

[23] A. Rosenqvist, C. Birket, E. Bartholome, and G. F. De Grandi, "Using satellite altimetry and historical gauge data for validation of the hydrological significance of the JERS-1 SAR (GRFM) mosaics in central Africa," in *Proc. IGARSS'99*, Hamburg, Germany, 1999, EE10_02.

[24] A. Rosenqvist, B. R. Forsberg, T. Pimentel, and J. E. Richey, "Using JERS-1 L-band SAR to estimate methane emissions from the Jau river floodplain," in *IEEE IGARSS'98*, Seattle, WA, July 6–10, 1998, pp. 1623–1625.

[25] F. De Grandi, P. Mayaux, J. P. Malingreau, A. Rosenqvist, S. Saatchi, and M. Simard, "New perspectives on global ecosystems from wide-area radar mosaics: Flooded forest mapping in the tropics," *Int. J. Remote Sensing: Special Issue on Global and Regional Land Cover Characterization from Satellite Data*.

[26] G. F. De Grandi, P. Mayaux, A. Rosenqvist, Y. Rauste, S. Saatchi, M. Simard, and M. Leysen, "Flooded forest mapping at regional scale in the central Africa congo river basin: First thematic results derived by ERS-1 and JERS-1 radar mosaics," in *Proc. Sec. Int. Workshop on Retrieval of Bio- and Geophys. Parameters from SAR Data, ESA ESTEC*, Oct. 21–23, 1998.

[27] S. Saatchi, G. F. De Grandi, M. Simard, and E. Podest, "Classification of JERS-1 image mosaic of central Africa using a supervised multi-scale classifier of texture features," in *Proc. IEEE IGARSS'99*, Hamburg, Germany, 1999, EE10-06.

[28] M. Simard, S. Saatchi, and G. F. De Grandi, "Classification of the Gabon SAR mosaic using a wavelet based rule classifier," in *Proc. IEEE IGARSS'99*, Hamburg, Germany, 1999, EE10-07.

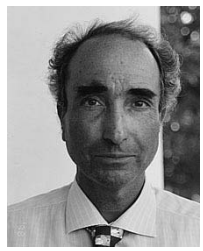

**Gianfranco (Frank) De Grandi** (M'90–SM'96) received the Ph.D. in physics engineering (with honors) from the Politecnico Milano, Milano, Italy, in 1973.

Since 1977, he has been with the European Commission Joint Research Centre (JRC), Ispra, Italy, where he has performed research in signal processing for application areas such as gamma ray spectroscopy, data communications, and radar remote sensing. In 1985, he was a Visiting Scientist with Bell Communications Research, Morristown, NJ, where he participated in the design of METROCORE, one of the first research projects for Gb rate metropolitan area networks. From 1986 to 1989, he headed the signal processing section of the Electronics Division, JRC, where he introduced VLSI design technology and conducted research, in cooperation with Bellcore, on packet video, and in cooperation with ITALTEL Italy on the European digital mobile phone network. In 1989, he joined the Institute for Remote Sensing Applications [now Space Applications Institute (SAI)], where he started a research activity in radar polarimetry in the Advanced Techniques unit. Since 1994, he has been Principal Scientist for radar remote sensing in the Global Vegetation Monitoring unit. Since 1997, he has been Assistant Professor with the Faculte' de Foresterie et Geomatique, Universite' Laval, Quebec, PQ, Canada. His current research interests span a wide gamut, including global scale forest mapping using high resolution spaceborne SAR, multiresolution analyses based on the wavelet representation for texture measures, backscattering multitemporal estimators, topography sensing using polarimetric SAR data, and the statistics of polarimetric synthesized SAR images.

Dr. De Grandi is a senior member of the IEEE Geoscience and Remote Sensing and Signal Processing Societies and a member of the Planetary Society, Pasadena, CA.

**Philippe Mayaux** received the engineer degree in agronomy and forestry in 1986, and the degree in land planning and the Ph.D. degree from the University of Louvain, Belgium, in 1999.

He has worked for several field projects in Tanzania and Senegal. Since 1995, he has been Coordinator for Africa within the European Commission Tropical Ecosystem Environment monitoring by Satellites (TREES) project. His work has focused on vegetation mapping at regional scale from optical and microwave data and on the problem of scaling in remote sensing. He is involved in many regional and global projects related to forest cover mapping, such as GRFM or GOFC.

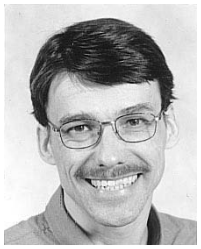

**Yrjo Rauste** was born in Espoo, Finland, in 1956. He received the M.S. degree in surveying and mapping in 1983 and the Licentiate of Technology in 1989, both from the Helsinki University of Technology, Espoo, Finland.

He has been with Technical Research Centre of Finland (VTT), Espoo, Finland, since 1979, except for visits to other research centers and his military service in 1983. From 1986 to 1987, he was a Visiting Scientist with the Institute for Image Processing and Computer Graphics, Graz Research Center, Graz, Austria. From 1997 to 1999, he was a postdoctoral grant holder with the Joint Research Centre (JRC), European Commission, Ispra, Italy. From 1994 to 1996, he also served as the Secretary of the Finnish Society of Photogrammetry and Remote Sensing. He is currently a Senior Research Scientist in the Remote Sensing group of VTT Automation. His research interests include application of SAR image analysis and processing (especially in forestry applications) and forest fire detection using optical satellite data.

**Ake Rosenqvist** received the M.Sc. degree from the Royal Institute of Technology, Stockholm, Sweden, in 1988, and the Ph.D. degree in civil engineering from the University of Tokyo, Tokyo, Japan, in 1997.

Since 1997, he has been a Visiting Scientist with the Joint Research Centre, European Commission (JRC SAI), Ispra, Italy, where he is involved in continental scale radar mapping of South America, Africa, and Siberia. He was an Invited Scientist with the National Space Development Agency of Japan (NASDA), Tokyo, Japan, from 1993 to 1997, where he was Project Scientist and Project Coordinator for the JERS-1 SAR Global Rain Forest and Boreal Forest Mapping Projects (GRFM/GBFM). From 1990 to 1993, he was with the Swedish Space Corporation, Stickholm, Sweden, focusing on Dem generation and land cover mapping by optical remote sensing.

Dr. Rosenqvist is currently the Chairman of the ISPRS working group for Global Monitoring (WG VII/5).

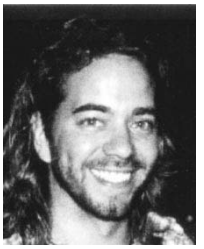

**Marc Simard** received the B.Sc. degree in physics (with honors) in astrophysics from Queen's University, Quebec, ON, Canada, in 1992, and the M.Sc. and Ph.D. degrees in physics (specializing in radioastrophysics) and geomatic sciences, respectively, from the Universite Laval, Quebec, in 1994 and 1998, respectively.

From 1995 to 1997, he was a Grant Holder with the Space Applications Institute of the Joint Research Center, European Communities (JRC SAI), Ispra, Italy. Since 1998, he has been a National Research Council Research Associate with the Jet Propulsion Laboratory, Pasadena, CA. His research interests include the multiscale analysis and classification of SAR images.

**Sasan S. Saatchi** received the B.S. and M.S. degrees in electrical engineering from the University of Illinois, Champaign, in 1981 and 1983 respectively, and the Ph.D. degree from the George Washington University, Washington, DC, in 1988 with a concentration in electrophysics and modeling of wave propagation in natural media.

From 1989 to 1991, he was a Postdoctoral Fellow, National Research Council, and worked at the Laboratory for Terrestrial Physics, NASA/Goddard Space Flight Center, Greenbelt, MD, on the hydrological application of active and passive microwave remote sensing. Since April of 1991, he has been a Scientist with the Radar Science and Engineering Section of the Jet Propulsion Laboratory, California Institute of Technology, Pasadena, CA, where he is involved in developing microwave scattering and emission models for soil and vegetated surfaces and retrieval algorithms for estimating geophysical parameters from spaceborne remote sensing instruments. He has been a Principal or Co-Investigator in several interdisciplinary international projects such as FIFE, EFEDA, Magellan, Mac-Hydro, Hapex-Sahel, BOREAS, LCLUC, and LBA. His present research activities include land cover classification, biomass and soil moisture estimation in boreal forests, land use and land cover change, and forest regeneration monitoring over tropical rain forests. His research interests also include wave propagation in disordered/random media and EM scattering theory.